Earth and Planetary Science Letters 531 (2020) 115927

Contents lists available at ScienceDirect

Earth and Planetary Science Letters

www.elsevier.com/locate/epsl

Anomalous structure of $MgCO_3$ liquid and the buoyancy of carbonatite melts

Sean M. Hurt [a,b,*], Aaron S. Wolf [a]

[a] Department of Earth and Environmental Sciences, University of Michigan, 1100 N. University Ave., Room 2534, Ann Arbor, MI 48109, USA
[b] Division of Math and Science, National Park College, 101 College Dr., Hot Springs National Park, AR 71913, USA

ARTICLE INFO

Article history:
Received 23 April 2019
Received in revised form 3 October 2019
Accepted 24 October 2019
Available online 13 November 2019
Editor: R. Dasgupta

Keywords:
$MgCO_3$ melt
carbonate liquid structure
carbonatite density
alkaline earth carbonates

ABSTRACT

$MgCO_3$ is one of the most important components of mantle-derived carbonatite melts, and yet also one of the most difficult to study experimentally. Attempts to constrain its thermodynamic properties are hampered by decarbonation, which occurs at only ~500 °C, far below its metastable 1 bar melting temperature. Molecular dynamic simulations, however, can predict the thermodynamic properties of the $MgCO_3$ liquid component in spite of experimental challenges. Using the recently developed empirical potential model for high-pressure alkaline-earth carbonate liquids (Hurt and Wolf, 2018), we simulate melts in the $MgCO_3$-$CaCO_3$-$SrCO_3$-$BaCO_3$ system from 773 to 2373 K up to 20 GPa. At 1 bar, $MgCO_3$ liquid assumes a novel topology characterized by a 4-fold coordination of the metal cation (Mg) with both the carbonate molecule and oxygen ion; this is distinct from the other alkaline-earth carbonate liquids in which the metal cation is in ~6- and ~8-fold coordination with carbonate and oxygen. With increasing pressure, $MgCO_3$ liquid structure becomes progressively more like that of (Ca, Sr, Ba)CO_3 liquids with Mg^{2+} approaching 6-fold coordination with carbonate groups. The novel network topology of $MgCO_3$ liquid results in a melt that is significantly more buoyant and compressible than other alkaline-earth carbonate liquids. Simulations of mixed $MgCO_3$-bearing melts show that metal cation coordination with O and C is independent of bulk composition. Mixed simulation also reveal that molar volume, compressibility, enthalpy and heat capacity do not mix ideally with (Ca, Sr, Ba)CO_3 liquids at 1 bar, a consequence of preferential metal-cation ordering in $MgCO_3$-bearing mixtures. As pressure increases, however, mixing progressively approaches ideality with respect to molar volume, becoming nearly ideal by 12 GPa. The model is further applied to mantle-derived primary carbonatite melts with compositions, temperatures and pressures determined by published phase equilibrium experiments. The voluminous structure of liquid $MgCO_3$ results in a buoyant melt that inhibits a density crossover with the surrounding mantle. Assuming $FeCO_3$ liquid also adopts the same anomalous high-volume structure as $MgCO_3$, we predict that even the most Fe-rich ferrocarbonatites would remain buoyant and be barred from sinking or stagnating in the mantle.

1. Introduction

Carbonate plays an important role in partial melting of the mantle. It can lower the solidus of mantle peridotite and eclogite up to ~600 °C (e.g. Dasgupta and Hirschmann, 2006; Hammouda, 2003), producing low degree partial melts of 0.03-0.3% carbonatite liquid (e.g. Green and Wallace, 1988; Dalton and Wood, 1993; Dasgupta and Hirschmann, 2006). Carbonatite liquids are highly mobile owing to their ultralow viscosities (e.g. Kono et al., 2014). They are efficient agents of metasomatism (e.g. Green and Wallace, 1988), are important for the petrogenesis of ocean island basalts (e.g. Dasgupta et al., 2006) and impact the deep carbon cycle (e.g. Dasgupta and Hirschmann, 2010).

Of all the carbonate liquid components, $MgCO_3$ is one of the most geologically relevant. Carbonate enters the mantle through subduction of hydrothermally altered oceanic crust (e.g. Staudigel et al., 1989). Calcium from $CaCO_3$ partitions readily into the silicate phases of the mantle and is replaced by Mg, establishing $MgCO_3$ as a dominant carbonate mantle component (Biellmann et al., 1993). Investigations into the composition of primary carbonatite melts produced by partial melting of carbonated mantle eclogite and peridotite show that $MgCO_3$ along with $CaCO_3$ and $FeCO_3$ are the major components of interest (Dalton and Wood, 1993; Dalton and Presnall, 1998; Hammouda, 2003; Ghosh et al., 2009).

* Corresponding author at: Division of Math and Science, National Park College, 101 College Dr., Hot Springs National Park, AR 71913, USA.
E-mail address: seanhurt@umich.edu (S.M. Hurt).

https://doi.org/10.1016/j.epsl.2019.115927
0012-821X/

Carbonated mantle systems have been extensively studied via phase equilibrium experiments (e.g. Dalton and Wood, 1993; Dalton and Presnall, 1998; Hammouda, 2003; Ghosh et al., 2009). While such experiments are immensely valuable, they have limitations. For example, small variations in the starting composition can result in marked changes to the location of the solidus in P-T space (Dasgupta and Hirschmann, 2010). This is problematic given the significant compositional heterogeneity of carbonated mantle, both in its silicate and carbonate phases. Compositional complexity is further compounded by wide ranges of temperatures and pressures where partial melting may occur. Phase equilibrium experiments cannot be performed for every relevant composition, temperature and pressure. Furthermore, experimenters often adjust temperature and pressure together, making it difficult to disentangle temperature- and pressure-effects.

Thermodynamic models such as MELTS (Ghiorso et al., 2002) or THERMOCALC (Powell and Holland, 1988) can help resolve these issues but they rely on knowledge of the standard state thermodynamic properties. For the most important carbonate crystal phases (e.g. magnesite, siderite and calcite), the standard state properties are well known (e.g. Berman and Brown, 1985). However, knowledge of the standard state thermodynamic properties of the respective liquids is limited because alkaline-earth carbonates and $FeCO_3$ decompose at temperatures lower than their 1 bar melting temperatures. In spite of the difficulties posed by decarbonation, some properties of the $CaCO_3$ liquid component have been determined experimentally such as 1 bar density and thermal expansion (e.g. Liu and Lange, 2003; Hurt and Lange, 2019) and 1 bar compressibility (O'Leary et al., 2015; Hurt, 2018). Some $CaCO_3$ liquid properties have also been determined at high pressure, such as the fusion curve (e.g. Li et al., 2017) and the high-pressure density and compressibility (Hudspeth et al., 2018). However, there is a notable absence of accurate determinations of the standard state thermodynamic properties of $MgCO_3$ and $FeCO_3$ liquid. This is due to the very low 1 bar decarbonation temperatures (only 500 °C for $MgCO_3$, Hurst, 1991), which makes experiments on $MgCO_3$ - and $FeCO_3$-bearing liquids nearly impossible at 1 bar.

At present, MD simulations provide the only plausible path for obtaining the complete set of carbonate liquid endmember properties needed to incorporate carbonate-silicate melting into a thermodynamic modeling framework like MELTS. The empirical potential model presented in Hurt and Wolf (2018) is designed specifically for simulations of alkaline-earth carbonate liquids at mantle conditions. In this study, we apply that model to simulate liquids in the $MgCO_3$-$CaCO_3$-$SrCO_3$-$BaCO_3$ quaternary system from 773 to 2373 K up to 20 GPa. The simulations supply crucial constraints on the standard state thermodynamic properties of $MgCO_3$ liquid which are difficult or impossible to determine experimentally. Apart from endmember thermodynamic properties, the simulations also explore liquid structure and mixing behavior in the $MgCO_3$-$CaCO_3$-$SrCO_3$-$BaCO_3$ quaternary system.

To assess whether carbonate melts are buoyant throughout the upper mantle and transition zone, simulations are also performed on $CaCO_3$-$MgCO_3$ binary compositions from 1.5 to 20 GPa and 1423 to 1873 K along various pressure-temperature paths approximating that of subducting slabs. The simulation composition, temperature and pressure are representative of near-solidus carbonatite melts formed by low-degree partial melting of carbonated eclogite and peridotite. This is done in order to estimate the density of primary carbonatite melts as a function of depth and determine whether any compositions of carbonate melt are sufficiently dense to either stagnate upon initial melting or sink into the lower mantle. Given the likely similarity of $MgCO_3$ and $FeCO_3$ liquid structures and volumes, we also explore the implications for ferrocarbonatite melts in the mantle.

2. Methods

For this study, we use a previously published empirical potential model for the simulation of alkaline-earth carbonate liquids using rigid ions and partial charges. A complete description of this model is available in (Hurt and Wolf, 2018) where it was applied to the simulation of liquids in the $CaCO_3$-$SrCO_3$-$BaCO_3$ system. This model is now applied to molecular dynamic (MD) simulations of $MgCO_3$-bearing liquids performed using the LAMMPS code (Plimpton, 1995).

While we use an empirical potential model, first-principles MD (FPMD) studies have made many significant contributions to the study of magmatic melts in recent years, including carbonated-silicate systems (e.g. Ghosh et al., 2017; Solomatova et al., 2019). Though FPMD is generally considered to provide more accurate estimates of interatomic forces than the empirical potential approach, FPMD simulations suffer from issues related to convergence, affecting the overall quality of simulated physical properties (e.g. Ganster et al., 2007). Empirical potential MD, when using well-trained potentials, can achieve results that are just as accurate as FPMD for bulk properties but at lower computational expense.

42 different liquid compositions are simulated within the $MgCO_3$-$CaCO_3$-$SrCO_3$-$BaCO_3$ quaternary over a temperature range of 773-2373 K and up to 20 GPa. These simulations extend to such low temperatures—well below the crystallization point for pure endmembers—because these carbonate liquids can be stable as important components within mixed composition liquids, which remain molten at much lower temperatures. MD simulations are performed with a timestep of 1 fs and total runtimes of 120 ps. Each simulation begins with an equilibration phase of 60 ps using the canonical (NVE) ensemble with the Berendsen barostat and thermostat (Berendsen et al., 1984), which equilibrates quickly and smoothly but deviates slightly from the canonical ensemble. A second equilibration phase of 40 ps is performed under the NPT ensemble using the Nosé-Hoover barostats and thermostats (Nosé, 1984; Hoover, 1985). A third phase of 20 ps continues the NPT ensemble and constitutes the final production run.

Every simulation is checked to ensure that system energies and volumes have converged to within 0.02% and 0.27%, respectively. This level of volume convergence is achieved with a simulation size of 6860 atoms. All simulations are initialized with atomic positions and velocities corresponding to $CaCO_3$ liquid at 2.275 g/cm^3 density (equivalent to 1 bar pressure) and 1623 K.

3. Results

3.1. Equation of state of $MgCO_3$ liquid

Hurt and Wolf (2018) previously showed that $CaCO_3$, $SrCO_3$ and $BaCO_3$ liquids have remarkably similar properties, with nearly parallel compression curves, 1 bar molar volumes that increase systematically with cation radius and congruent thermal expansions. Such systematic variation in molar volume and congruent thermal expansions are corroborated by the experiments of Hurt and Lange (2019) and Hurt (2018). Simulated compression curves for (Ca, Sr, Ba)CO_3 liquids are shown in Fig. 1 (solid lines), together with a hypothetical curve representing the expected behavior for $MgCO_3$ liquid (dotted line) assuming it follows the systematic trend of the other alkaline-earth carbonates.

To investigate whether $MgCO_3$ liquid follows the trends observed among $CaCO_3$, $SrCO_3$ and $BaCO_3$, its thermodynamic properties of $MgCO_3$ have been calculated from MD simulations (complete details and results are listed in Table A.1). Following Hurt and Wolf (2018), we attempt to fit the $MgCO_3$ simulation results with a temperature-dependent 3rd order Birch-Murnaghan equation of state (EOS), but the resulting models show a markedly poor fit to

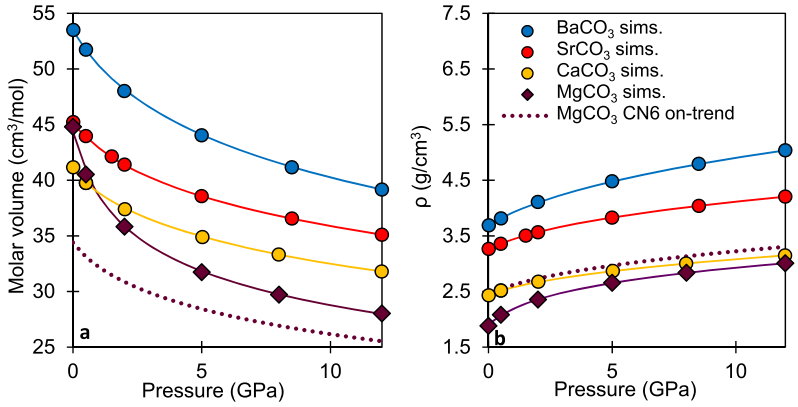

Fig. 1. Compression curve of $MgCO_3$ liquid strongly deviates from expectations based on the other alkaline-earth carbonates. Panel a shows simulated molar volumes at 1100 K as a function of pressure for $MgCO_3$, $CaCO_3$, $SrCO_3$ and $BaCO_3$ liquids. Points show simulation results, while solid lines represent best-fit Birch-Murnaghan EOS for each liquid (3rd order for $CaCO_3$, $SrCO_3$ and $BaCO_3$ and 4th order for $MgCO_3$). The dotted line represents the expected compression curve of $MgCO_3$ if its volumetric properties were in-line with periodic trends observed among the other alkaline earth carbonates (i.e. if Mg-C coordination was 6-fold rather than 4). As evident, $CaCO_3$, $SrCO_3$ and $BaCO_3$ form nearly parallel curves that increase systematically from Ca to Ba, while $MgCO_3$ liquid deviates dramatically, especially at low pressure. Panel b shows the same compression curves in terms of density.

Table 1
The thermodynamic properties of $MgCO_3$ liquid as derived from the simulations. These are fitted parameters of both a 3rd and 4th order Birch-Murnaghan EOS (Eqs. A1-A4) that have been fitted to the simulations of $MgCO_3$ liquid from 773 to 2000 K up to 20 GPa by the least squares method. $V_{Tr,0}$ is the molar volume at 1100 K and 1 bar; α is the thermal expansion; $K_{Tr,0}$ is the bulk modulus at 1 bar and 1100 K and $\delta K_0/\delta T$ is its temperature dependence; K' and K'' are first- and second-pressure derivatives of the bulk modulus. The root mean square of the pressure residuals of the 4th order fit is 0.06 GPa and of the volume residuals is 0.27 cm^3/mol.

Property	Best Fit (1σ)	
	3rd order EOS	4th order EOS
RMS Press. residual (GPa)	0.11	**0.06**
$V_{Tr,0}$ (cm^3/mol)	46.0(2)	**44.21(9)**
α ($10^{-4}\cdot$ K^{-1})	0.004(13)	**1.07(14)**
$K_{Tr,0}$ (GPa)	0.9(20)	**6.15(15)**
$\delta K_0/\delta T$ ($10^{-3}\cdot$ GPa/K)	−0.1(18)	**−1.37(35)**
K'	33(75)	**2.41(1)**
K''		**3.16(1)**

the data, reflected in both large pressure residuals and large error bars on the fitted parameters (Table 1). Unlike (Ca, Sr, Ba)CO_3 liquids, $MgCO_3$ liquid is highly compressible at pressures <2 GPa and its rapid change in molar volume cannot be accommodated by a 3rd order Birch-Murnaghan, thus requiring us to adopt a 4th order Birch-Murnaghan EOS (details of the EOS are available in Appendix A).

The full set of parameters for this EOS is given in Table 1. This 4th order Birch-Murnaghan EOS model recovers the simulated molar volumes in the 1100 – 2000 K temperature range up to 20 GPa with RMS volume residuals of 0.27 cm^3/mol (0.81%). The 1100 K compression curve predicted by this best-fit EOS model is shown in Fig. 1 along with the raw simulated molar volume data as a function of pressure up to 12 GPa. Our simulation results predict radically different compression behavior for $MgCO_3$ as compared to the expected compression curve based on the other three alkaline-earth carbonate components. The 1 bar molar volume is near that of $SrCO_3$ and decreases dramatically with pressure, implying a 1 bar compressibility far-exceeding that of the other alkaline-earth carbonate liquids. The compression curve rapidly flattens out and begins to parallel the other alkaline-earth carbonates at pressures > 5 GPa. The thermophysical properties of liquids derive from their average atomic structure, and thus we explore the pressure-dependent atomic structure of $MgCO_3$ liquid to discover the root cause for this unique behavior among the alkaline-earth carbonates.

3.2. Distinct structure of $MgCO_3$ liquid

Though liquids lack long-range order, they do possess short-range order that can be described using a pair distribution function (pdf). For a particular pair of atomic types (i and j), pdf curves give the average density of j atoms as a function of distance from atom i. Liquid structure can also be described by coordination numbers for a given atomic pair. Average coordination numbers are calculated as weighted averages of the pdf curves, $g_{ij}(r)$:

$$CN_{ij} = 4\pi \int_0^{r_1} r^2 g_{ij}(r)\, \rho_j \, dr \qquad (1)$$

where r is the atomic separation distance, ρ_j is the average atomic number density of atom j, and r_1 is the maximum cutoff radius located at the first minimum in the PDF, representing the outer boundary of the first nearest-neighbor peak.

Hurt and Wolf (2018) used the same empirical potential model to simulate (Ca, Sr, Ba)CO_3 liquids, and demonstrated that they have remarkably similar liquid structures and coordination numbers for the metal-oxygen (M-O), carbon-carbon (C-C) and metal-carbon (M-C) pairs. At ambient pressure, C-C and M-C coordination numbers are the same for each liquid at 10.9 and 5.9 respectively. M-O coordination numbers are similar for the three endmember liquids, increasing systematically from Ca to Ba (Ca-O: 6.9, Sr-O: 7.3 and Ba-O: 7.7).

Based on the new simulations performed in this study, we analyze the structure of $MgCO_3$ liquid. The 1 bar results are summarized in Fig. 2, which shows a distinctly different atomic structure and coordination environment for $MgCO_3$ as compared to the other alkaline-earth carbonate liquids, visible in terms of C-C, M-O and M-C pairs. See Appendix C and Fig. C.3 for the detailed coordination distributions of all alkaline-earth liquids across a range of P-T conditions. At 1 bar and 1100 K, the Mg-O and Mg-C coordination is fourfold. The average value of 4.0 is distributed with 43% of Mg-O pairs in 4-fold coordination while 17% and 27% are in 3- and 5-fold coordination (the remaining pairs are divided among 2- and 6-fold). C-C coordination (11.6) is nearly ideal closest-packing, similar to $CaCO_3$-$SrCO_3$-$BaCO_3$ liquids which adopt slightly lower values (10.6-11.3). The most significant and systematic difference for the alkaline-earth carbonates is seen in the M-C pairs. The

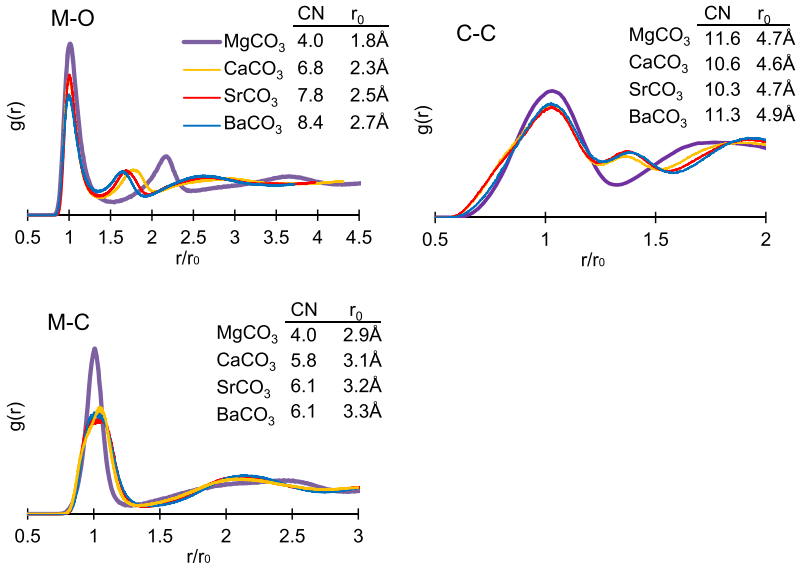

Fig. 2. Liquid structure of $MgCO_3$ is distinct from $CaCO_3$, $SrCO_3$ and $BaCO_3$. Pair distribution functions are calculated from liquid simulations at 1 bar and 1100 K for atomic pairs between carbon (C), oxygen (O) and metal cations (M: Mg, Ca, Sr, Ba). The M-O, C-C and M-C pairs shown in panels a, b and c, respectively. For visual comparison, interatomic separation distance (r) has been normalized to the position of the first peak (r_0). Average coordination number (CN) has been calculated for each pair in the embedded tables. (For interpretation of the colors in the figure(s), the reader is referred to the web version of this article.)

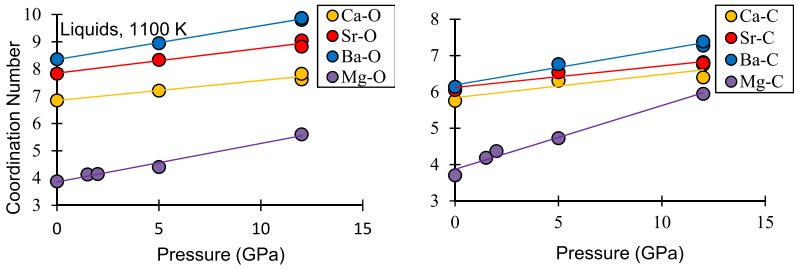

Fig. 3. The structure of $MgCO_3$ liquid becomes progressively more like (Ca, Sr, Ba)CO_3 liquids at high pressure. The simulated evolution of coordination for M-O and M-C pairs (in panels a and b), is shown for pure $MgCO_3$, $CaCO_3$, $SrCO_3$ and $BaCO_3$ liquids as a function of pressure up to 12 GPa. In $MgCO_3$, the coordination of M-O and M-C pairs starts at 4 at 1 bar and approaches ~6 at 12 GPa (while other alkaline earths' coordination evolution is more modest, rising 2-4 times slower).

average CN for M-C pairs is between 5.8 and 6.1 for the other alkaline-earth carbonate liquids, but is only 4.0 for $MgCO_3$—the same as in alkali carbonates (e.g. Roest et al., 2017). These differences are also mirrored in the coordination distributions, which show a dramatically narrower range of values for $MgCO_3$ compared to the other alkaline-earth carbonates. The standard deviation (average width) of the CN distribution for $MgCO_3$ at 1 bar is 0.46, nearly half that of the remaining alkaline-earth carbonates, which all show a width of 0.90 (Fig. C.3 in the Appendix).

To determine whether the unique structure of $MgCO_3$ liquid persists at high pressure, isothermal compression simulations are analyzed at 1100 K between 1 bar and 12 GPa. M-C and M-O coordination numbers are calculated at each pressure and shown in Fig. 3. As pressure increases, the average Mg-O coordination number increases linearly from 4 (at 1 bar) to 5.6 (at 12 GPa). In the high-pressure regime, M-O coordination number adopts systematic behavior among the alkaline-earth carbonates: the average coordination number is ~10 for Ba-O, ~9 for Sr-O, ~8 for Ca-O and ~6 for Mg-O. Thus, at pressure, the Mg-O coordination number is consistent with what might be expected from periodic systematics. For the M-C coordination numbers, $CaCO_3$-$SrCO_3$-$BaCO_3$ liquids average around 6 at 1 bar and then increase modestly to ~6.8 by 12 GPa. For $MgCO_3$, the Mg-C coordination starts off at 4.0 at 1 bar and converges rapidly to values consistent with the other alkaline-earth carbonates (~6). While the average 1 bar coordination of the typical alkaline-earth carbonate liquids is 6.0, not a single Mg-C pair is in 6-fold coordination within $MgCO_3$; by 5 GPa, ~30% of the Mg-C pairs are 6-fold coordinated. Simulations thus indicate that the liquid structure of $MgCO_3$ becomes progressively more like that of the other alkaline-earth carbonates with compression, becoming nearly indistinguishable by 12 GPa.

3.3. *Non-ideal mixing for $MgCO_3$ liquid at low pressure*

Hurt and Wolf (2018) simulated alkaline-earth carbonate liquids in three binary systems: $CaCO_3$-$SrCO_3$, $CaCO_3$-$BaCO_3$ and $SrCO_3$-$BaCO_3$. It was found that molar volumes and molar isobaric heat capacities and compressibility all mix ideally across a wide range of temperatures and pressures. To test whether such ideal mixing behavior extends to $MgCO_3$-bearing liquids, simulations of mixed liquids are performed in the $MgCO_3$-$CaCO_3$-$SrCO_3$-$BaCO_3$ quaternary system at 1 bar and 1100 K. For any property of interest, we define the mixing quantity as the deviation from a compositionally-weighted average of the endmembers:

$$\Delta Z_{mix} = Z - \sum Z_i X_i \tag{2}$$

where Z is the molar quantity of interest (like volume or enthalpy) for the liquid mixture, X_i is mol fraction of each endmember, and Z_i is the quantity for each pure endmember at the specified temperature and pressure. The ideality of mixing in terms of both volume and enthalpy is assessed for simulated Mg-carbonate bina-

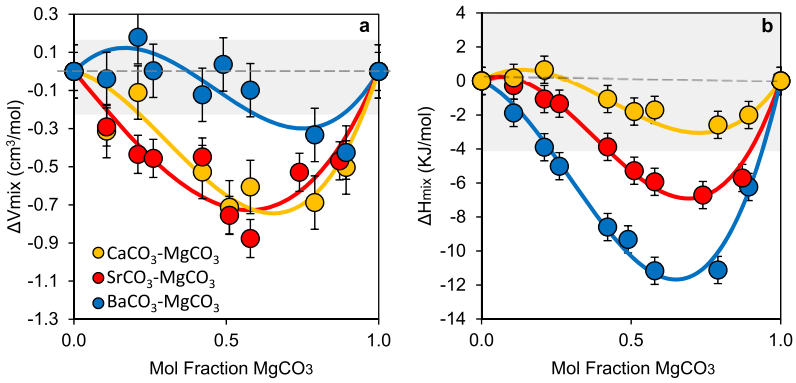

Fig. 4. Non-ideal mixing dominates volumetric and enthalpic properties in $MgCO_3$-bearing systems at 1 bar. The ΔV_{mix} (a) and ΔH_{mix} (b) of $MgCO_3$-bearing binary liquids at 1100 K and 1 bar are shown, with non-zero values indicating non-ideal mixing. The shaded regions reflect the range of ΔV_{mix} and ΔH_{mix} for the ideal mixing of (Ca, Sr, Ba)CO_3 liquids calculated by Hurt and Wolf (2018). Both ΔV_{mix} and ΔH_{mix} are, for the most part, negative and reach a minimum at $MgCO_3$ molar concentrations of 0.6 to 0.8. Points show simulation results and lines are the best-fit sub-regular solutions (Eq. (3)). Note that, for ΔH_{mix}, simulated total energy values are used instead of enthalpy because they are equal at 1 bar and because simulated total energy has smaller errors than enthalpy due to random fluctuations in both pressure and volume.

ries and visualized in Fig. 4 (with direct simulation results reported in Appendix Table C.2).

Properties determined from MD simulations always contain uncertainties due to random fluctuations and system size limitations. We can reduce the effects of this noise and better characterize non-ideal mixing by fitting a simple sub-regular mixing model to the simulated ΔV_{mix} and ΔH_{mix} values:

$$\Delta Z_{mix} = \left(w + \Delta w \left[X - \frac{1}{2} \right] \right) \cdot X[1 - X] \tag{3}$$

where ΔZ_{mix} is the mixing property for either volume or enthalpy, X is mol fraction of $MgCO_3$, and w and Δw are constants which have been fitted using least squares minimization. The best-fit values of w and Δw at 1100 K and 1 bar for all three binaries are given in Appendix Table C.3. Fig. 4 depicts ΔV_{mix} in panel a and ΔH_{mix} in panel b for each simulated mixture as a function of $MgCO_3$ content along with the best-fit sub-regular solution model (Eq. (3)). Fig. 4a shows significant non-ideal volume of mixing for all binaries, especially along the $CaCO_3$-$MgCO_3$ binary where ΔV_{mix} is as large as $-0.87 \pm .11$ cm^3/mol. Volumes of mixing are nearly all predicted to be negative. For all binaries, the mixing behavior is slightly asymmetric; the magnitude of ΔV_{mix} reaches a maximum at 60-75 mol% $MgCO_3$. The non-ideal mixing of volumes in $MgCO_3$-bearing liquids means that volumetric derivative properties such as compressibility also cannot mix ideally.

The case of enthalpy of mixing (ΔH_{mix}) is closely analogous. Unlike liquids in the $CaCO_3$-$SrCO_3$-$BaCO_3$ system, enthalpy does not mix ideally among $MgCO_3$-bearing mixtures. Fig. 4b shows that ΔH_{mix} is uniformly negative or statistically consistent with zero across the binary for every mixture. The peak magnitude of ΔH_{mix} increases systematically from $CaCO_3$ (31 KJ/mol) to $BaCO_3$ (~12 KJ/mol). Within each binary, the magnitude of ΔH_{mix} peaks at 60-75 mol% $MgCO_3$. Interestingly, the $BaCO_3$-$MgCO_3$ system exhibits the lowest ΔV_{mix} but the highest ΔH_{mix}; this suggests that the mechanism responsible for non-ideal mixing in volumetric properties is not the same as the one driving non-ideal mixing in enthalpic properties.

Hurt and Wolf (2018) found that simulations predict isobaric heat capacities to mix ideally according to mol fraction in $CaCO_3$-$SrCO_3$-$BaCO_3$ liquids. Simulations in this study of $MgCO_3$-bearing binary liquids from 1100 to 2000 K enabled calculation of the isobaric 1 bar heat capacity. For $CaMg(CO_3)_2$, $SrMg(CO_3)_2$ and $BaMg(CO_3)_2$, the heat capacity is estimated to be 146, 140 and 139 J/mol, which are lower than their ideal values by 7%, 11%, and 9%, respectively. Heat capacities are thus systematically lower (9% on average) than expected for $MgCO_3$-bearing-systems.

3.4. Ideal mixing of $MgCO_3$ liquid at high pressure

Though its structure and compressive properties are distinct at low pressures, $MgCO_3$ liquid increasingly resembles other alkaline-earth carbonates at higher pressures. This is apparent in the compression curves, which become nearly parallel between 5 and 10 GPa as shown in Fig. 1. To further investigate, binary mixture simulations of $CaMg(CO_3)_2$, $SrMg(CO_3)_2$ and $BaMg(CO_3)_2$ are also performed at 1100 K up to 12 GPa, assessing whether volumes and enthalpies mix ideally at pressure. The values of ΔV_{mix} calculated from the resulting simulations are $-0.02 \pm .03$, $-0.13 \pm .03$ and $-0.11 \pm .03$ cm^3/mol for $CaMg(CO_3)_2$, $SrMg(CO_3)_2$ and $BaMg(CO_3)_2$ respectively. These ΔV_{mix} values are dramatically smaller than at 1 bar (which range between -0.34 and -0.91 cm^3/mol). Fig. 5 shows the compression behavior of ΔV_{mix} at 1100 K, normalized to the pressure-dependent absolute volume difference between $CaCO_3$ and $MgCO_3$ liquid, $\Delta V_{MgCO_3\text{-}CaCO_3}$. This pressure-dependent normalization is necessary since the molar volume of the $MgCO_3$-$CaCO_3$ binary mixture falls between the volumes of the pure endmembers, and thus at pressures where pure $CaCO_3$ and $MgCO_3$ volumes converge, ΔV_{mix} will appear small; normalizing to the volume difference between the endmembers corrects for this. As seen in the figure, ΔV_{mix} approaches 0 as pressure increases, reflecting increasingly ideal mixing.

At low pressures, metal-cation ordering provides a mechanistic explanation for non-ideal mixing of at least some of the properties in $MgCO_3$-bearing liquids (see Appendix C for a full discussion). Since ΔV_{mix} diminishes to nearly 0 at 12 GPa, we might expect to see little difference between Mg-Mg pdf curves in pure $MgCO_3$ versus $MgCO_3$ mixtures at that pressure. The inset on Fig. 5 shows, in fact, that the structural difference between pure and mixed $MgCO_3$ liquids progressively lessens with pressure (up to 12 GPa), supporting the notion that metal cation ordering correctly explains non-ideal mixing in volumetric properties among $MgCO_3$-bearing liquids.

In contrast, the simulations indicate that non-ideal mixing of enthalpy does not disappear at high pressure like ΔV_{mix}. At 12 GPa, ΔH_{mix} for $CaMg(CO_3)_2$, $SrMg(CO_3)_2$ and $BaMg(CO_3)_2$ is calculated to be -2.9, -8.2 and -11.7 kJ/mol respectively. Normalizing ΔH_{mix} to the difference in enthalpy between the endmembers would yield a more meaningful comparison (since absolute values of enthalpy increase with pressure). This result gives a normalized ΔH_{mix} of -1.2%, -2.1% and -1.9% at 12 GPa compared to -1.1%, -1.8% and -4.5% at 1 bar for $CaMg(CO_3)_2$, $SrMg(CO_3)_2$ and $BaMg(CO_3)_2$, respectively. $BaMg(CO_3)_2$ is the only mixture that undergoes a significant reduction in ΔH_{mix} with pressure, while the

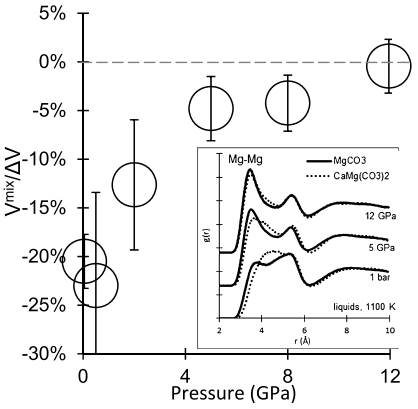

Fig. 5. Mixing of molar volumes for $CaCO_3$ and $MgCO_3$ liquid approach ideality with increasing pressure due to a progressively diminishing cation ordering effect. V_{mix} is shown as a function of pressure normalized to $\Delta V_{Ca\text{-}Mg}$ (which is the difference between pure $CaCO_3$ and $MgCO_3$ liquid at the given pressure). As pressure increase, the magnitude of non-ideality approaches 0. The figure inset shows corresponding liquid Mg-Mg pdf curves of pure $MgCO_3$ (solid lines) and $CaMg(CO_3)_2$ (dotted lines) at 1 bar, 2 and 12 GPa. The disparity between the two curves reflects the degree of cation ordering in the liquid. As pressure increase, the mixed $CaMg(CO_3)_2$ curve conforms to that of pure $MgCO_3$.

normalized ΔH_{mix} for the other binary liquids remain unchanged. This suggests that cation ordering in $MgCO_3$-bearing liquids is not solely responsible for non-ideal mixing of enthalpies.

3.5. Mg coordination in $MgCO_3$-bearing liquid mixtures

In addition to analyzing bulk properties, we also explore the atomic structures of Mg-bearing mixtures across a wide range of compositions. One of the most important results that emerged from these multicomponent simulations is that Mg-O and Mg-C coordination is insensitive to bulk composition. This means that, Mg^{2+} retains its fourfold coordination with oxygen and carbonate even in mixtures, revealing how the structure and properties of pure $MgCO_3$ provide a window into the behavior of geologically-relevant melts. The full range of pdf curves for M-O, M-C and C-C pairs for all binary compositions are available in Appendix Fig. C.1. The striking uniformity of pdf curves demonstrates how M-O, M-C and C-C pairs in binary liquids retain the same structure and coordination as in the pure liquids. Similarly, if small amounts of $CaCO_3$, $SrCO_3$ and $BaCO_3$ are mixed into $MgCO_3$ liquid, Ca^{2+}, Sr^{2+} and Ba^{2+} ions maintain their octahedral coordination with carbonate.

This is an important result because the anomalous properties of $MgCO_3$ liquid are most pronounced at low pressure where pure $MgCO_3$ does not melt congruently. While pure $MgCO_3$ liquid is not stable at 1 bar, it is stable as a component in a mixed liquid, for example, $K_2Mg(CO_3)_2$ (Sharma and Simons, 1980). Our simulations show that, while mixing between $MgCO_3$ and the other alkaline-earth carbonates is not perfectly ideal, it is sufficiently close to yield useful estimates of its partial molar properties based on its pure-liquid properties.

4. Discussion

4.1. Fourfold cation coordination in $MgCO_3$ liquid at 1 bar

Previous molecular dynamic studies have found that most alkaline-earth carbonate liquids ($CaCO_3$, $SrCO_3$, $BaCO_3$) adopt similar 1 bar atomic structures, with metal cations in octahedral coordination with carbonate anions and 7-8 fold coordination with oxygen (e.g. Hurt, 2018; Vuilleumier et al., 2014). A thorough search of the literature reveals, to the best of our knowledge, that this study is the first to demonstrate that $MgCO_3$-bearing melts are unique among those of the alkaline-earth carbonates, with Mg in an average fourfold coordination with both oxygen and carbonate anions. This structural anomaly is all the more surprising, given that Mg-bearing carbonate crystals (magnesite, dolomite, huntite, and northsite) all possess 6-fold oxygen coordination.

In silicate crystals, Mg is also mostly in 6-fold coordination with oxygen, the only exceptions being spinel and åkermanite ($Ca_2Mg[Si_2O_7]$) which host Mg in fourfold coordination with O (e.g. Kroeker and Stebbins, 2000). While Mg is mostly found in 6-fold coordination with O in solid silicate phases, it is possible for it to enter near 4-fold coordination upon melting, opening the door for similar behavior in carbonate systems. A good example of this behavior can be found in the crystal enstatite (Mg_2SiO_6), where Mg-O coordination is 6-fold but decreases to 4.35 in the liquid (Cormier and Cuello, 2013).

In silicate melts and glasses an average Mg-O coordination number of 4.0 is rarely observed. However, Mg-O coordination numbers of <5 have been observed across a wide range of compositions in silicate melts and glasses (e.g. Roy, 1950; Waseda and Toguri, 1977; Kubicki et al., 1992; Shimoda et al., 2008; Trcera et al., 2009; Cormier and Cuello, 2013). Karki et al. (2018) performed FPMD simulations of silicate melts with compositions representing mid-ocean ridge basalt and found an average Mg-O coordination of 4.62; Guillot and Sator (2007) similarly performed classical MD simulations on systems analogous to peridotite and found and average Mg-O coordination of 4.8. It should be noted that, while common, Mg does not always assume such a low coordination state in all silicate melts and glasses. For example, at 1 bar, Morizet et al. (2019) found an average Mg-O coordination of 5- to 6-fold from X-ray and neutron diffraction experiments on CO_2-bearing silicate glasses.

The average Mg-O coordination in carbonate melts is unfortunately difficult to assess from past analytical studies. Detailed structural information on Mg^{2+} coordination in $MgCO_3$-bearing carbonate melts/glasses is largely unavailable. This is in part because melt structure is commonly determined via experimental analyses of glasses (such as XANES or EXAF), and while silicate melts readily quench to glass, there is only one purely carbonate system that is capable of vitrification: K_2CO_3-$MgCO_3$ (e.g. Datta et al., 1964; Ragone et al., 1966). This system is doubly unique because it is the only known $MgCO_3$-bearing carbonate liquid that forms a stable melt at 1 bar (Ragone et al., 1966). K_2CO_3-$MgCO_3$ glass structures have been studied by both infrared (Datta et al., 1964; Genge et al., 1995) and Raman spectroscopy (Sharma and Simons, 1980; Genge et al., 1995). Neither Genge nor Sharma comment on Mg^{2+} coordination in their spectroscopic studies. However, Datta et al. (1964) posited that the low refractive index and density of the K_2CO_3-$MgCO_3$ glass (compared to the respective crystals) may result from a low (4-fold) Mg coordination. Datta also recognized the significance of the fact that the only known $MgCO_3$-bearing carbonate liquid that is stable at 1 bar is also the only carbonate capable of quenching to a glass, implying its structure must somehow be unique among alkaline-earth carbonate liquids; Datta thus hypothesized that it could be related to a decrease in Mg^{2+} coordination number. Our MD simulations suggest that $MgCO_3$ liquid does in fact assume a unique topology characterized by a low (4-fold) coordination of Mg^{2+}, which corroborates the suppositions of Datta et al. (1964) on the structure of $MgCO_3$-bearing carbonate melts.

4.2. Comparison of $MgCO_3$ to other alkaline-earth carbonate liquids

From the simulations of this study, it appears that $MgCO_3$ has a liquid structure that is distinct from the other alkaline-earth carbonates and properties that deviate strongly from those predicted

on the basis of systematic variations (see Hurt, 2018; Hurt and Lange, 2019). Hurt and Lange (2019) explored systematic variations in the 1 bar molar volumes of alkali and alkaline-earth carbonate liquids. On the basis of systematic trends, two different estimates of $MgCO_3$ liquid molar volume were made; one estimate assumes that the CN of Mg-C and Mg-O are both 6 and has a liquid structure that is like the other alkaline-earth carbonates. The other estimate assumes the CN of Mg-O and Mg-C is 4 and has a liquid structure that is more like an alkali carbonate. Under the 6-fold assumption, Hurt and Lange predict a 1 bar $MgCO_3$ liquid molar volume of $34.4 \pm .6$ cm^3/mol. In the case of a 4-fold Mg-O coordination, Hurt and Lange (2019) estimated that $MgCO_3$ would have a 1 bar liquid molar volume of $\sim$40 cm^3/mol at 1100 K.

Our simulations clearly predict 4-fold coordination for Mg^{2+} and a liquid structure that is more like alkali carbonate than typical alkaline-earth carbonates (a full discussion of similarities between $MgCO_3$ and alkali carbonate liquid structure is available in Appendix B). In accordance with the estimates of Hurt and Lange (2019), our simulations predict a larger 1 bar molar volume than what might be expected from systematic variations in the molar volumes of alkaline-earth carbonate liquids. The fitted Birch-Murnaghan EOS model (Appendix Eq. A.1-A.4) predicts a 1 bar $MgCO_3$ liquid volume of $44.21 \pm .09$ cm^3/mol at 1100 K. However, it's likely that the actual volume is somewhat lower since the empirical potential model of Hurt and Wolf (2018) typically slightly overestimates 1 bar volumes. For $CaCO_3$, $SrCO_3$ and $BaCO_3$ liquids, the model requires a -0.35, -0.33 and -0.75 GPa pressure correction, respectively, to bring simulated 1 bar volumes into agreement with the experimental projections of Hurt and Lange (2019). An analogous -0.6 GPa pressure correction would bring the $MgCO_3$ simulations into agreement with the alkali-like structural predictions from Hurt and Lange (2019).

Hurt (2018), provides analogous systematic trend equations for the compressibility of alkali and alkaline-earth carbonate liquids based on a positive linear relationship between liquid compressibility and volume of fusion. Their model equation predicts a compressibility for $MgCO_3$ liquid at 1100 K of $\sim 23 \pm 1$ 10^{-2} GPa^{-1}, assuming it fits into the alkali carbonate trend, and $\sim 18 \pm 6$ 10^{-2} GPa^{-1} if it fits into the alkaline-earth trend. Given the similarity of the $MgCO_3$ liquid structure to Li_2CO_3 (Appendix Fig. B.1), the alkali carbonate trend might actually provide a better prediction (for more details regarding similarities between $MgCO_3$ and alkali carbonates, see Appendix B). These estimates of $MgCO_3$ liquid compressibility differ dramatically from other alkaline-earth carbonate liquids (i.e. $CaCO_3$, $SrCO_3$ and $BaCO_3$) which have relatively modest 1 bar/1100 K compressibilities of 4.33 - 5.97 $\cdot 10^{-2}$ GPa^{-1}. Our $MgCO_3$ liquid simulations predict a bulk modulus (K_T) of $6.15 \pm .15$ GPa, which is equivalent to a compressibility (β_T) of $16.3 \cdot 10^{-2}$ GPa^{-1} at 1100 K, broadly consistent with the elevated values predicted by Hurt (2018).

4.3. Comparison to previous thermodynamic studies of $MgCO_3$ liquid properties

As noted above, the structure of $MgCO_3$ liquid becomes more like the other alkaline-earth carbonates with greater pressure. By 12 GPa, the Mg-O and Mg-C coordination converge to values in line with $CaCO_3$, $SrCO_3$, and $BaCO_3$ liquids (Fig. 2). This pressure-induced transformation of liquid structure is also evident in the compression curve of $MgCO_3$ liquid, which begins to parallel the other three alkaline-earth carbonate liquids at 5-10 GPa (Fig. 1).

Our predictions of the standard state thermodynamic properties of $MgCO_3$ liquid stand in stark contrast to previous estimates made by Kang et al., 2016. These calculations fit a thermodynamic model to the congruent melting curve of $MgCO_3$, which is bracketed by four experimentally determined points ($\sim$1858 K at 3 GPa & 1883 K at 3.6 GPa from Irving and Wyllie, 1975, and 2183 K at 8 GPa & 2363 K at 15 GPa from Katsura and Ito, 1990). This approach arrives at a molar volume of $MgCO_3$ liquid of $\sim$32 cm^3/mol and a compressibility of $2.6 \cdot 10^{-2}$ GPa^{-1} at 1100 K and 1 bar. While the $MgCO_3$ properties proposed by Kang et al. differ markedly from our simulation results, Kang et al. arrived at their values using a method that is statistically problematic. The estimates of standard state thermodynamic properties of $MgCO_3$ liquid (and $FeCO_3$ as well) proposed by Kang et al. were calculated by fusion curve analysis. The fusion curve of $MgCO_3$ is currently bracketed by 4 experimental points (and only 3 for $FeCO_3$). However, 5 thermodynamic parameters are fitted to each dataset. Since the number of fitted parameters exceeds the number of constraining observations, the reported thermodynamic solution is highly under-constrained and non-unique, allowing alternative sets of thermodynamic properties to perfectly recover the limited observables.

We can see some of the resulting issues directly in the fitted thermodynamic properties proposed by Kang et al. (2016); for example, Kang gives thermal expansions of $MgCO_3$ and $FeCO_3$ liquid that are identical to the thermal expansion of their respective crystal phases. However, the thermal expansion of a liquid is generally expected to be substantially greater than that of the crystal (e.g. Lange, 1997). $CaCO_3$, $SrCO_3$ and $BaCO_3$ liquids, for example, have thermal expansions $\sim$3 times greater than their respective crystal phases (Hurt and Lange, 2019). Kang et al. also give a temperature dependence of compressibility ($\delta\beta_T/\delta T$) of $MgCO_3$ liquid that is lower, by an order of magnitude, than those of $CaCO_3$, $SrCO_3$ and $BaCO_3$ liquids (Hurt, 2018). For these reasons, we strongly recommend the standard state $MgCO_3$ liquid thermodynamic properties derived from this study.

4.4. The density of primary carbonatite melts

Natural carbonatite liquids have been shown to be effective agents of mantle metasomatism and scavengers of trace elements (e.g. Blundy and Dalton, 2000), and thus the mobility and ascent rates of primary carbonatite melts are particularly important. Ascent rate depends mostly on melt viscosity and density contrast. Viscosity has been measured at temperatures and pressure representative of the mantle for calcitic and dolomitic liquids (e.g. Kono et al., 2014); and the density of $CaCO_3$ liquid has been determined experimentally at 1 bar (e.g. Hurt and Lange, 2019) and at high-pressure (Hudspeth et al., 2018). However, primary carbonatite melts generated in the mantle by low-degree partial melting contain significant amounts of $MgCO_3$ and $FeCO_3$ (e.g. Dalton and Wood, 1993; Ghosh et al., 2009).

While the densities of primary carbonatite melts along a carbonated mantle liquidus are mostly unknown, it may be estimated by simulations from this study. Using the compositions of low-degree primary carbonatite melts generated in phase equilibrium experiments of carbonated peridotite and eclogite (Dalton and Wood, 1993; Dalton and Presnall, 1998; Hammouda, 2003; Ghosh et al., 2009), simulations at temperature and pressure are performed for simplified experimental compositions by projecting them into the $CaCO_3$-$MgCO_3$ binary. Complete details on these calculations are available in Appendix D.

The simulated density results are listed in Table 2 and depicted as a function of depth in Fig. 6. The simulations indicate that $CaCO_3$-$MgCO_3$ binary liquids will be relatively low in density due to the open network topology of the $MgCO_3$ melt component. Thus, primary carbonatite melts maintain a significant density contrast with the surrounding mantle rocks throughout the entire upper mantle and transition zone. Even the densities of melts from Hammouda (2003), which represent a cold slab subduction PT path (and are relatively enriched in denser $CaCO_3$ and $FeCO_3$ components) never approach that of the mantle. Given the ultralow vis-

Table 2
Simulated densities of (Ca, Mg)CO_3 binary liquids approximating compositions of carbonatite melts from phase equilibrium experiments of carbonated mantle (Dalton and Wood, 1993; Dalton and Presnall, 1998; Hammouda, 2003; Ghosh et al., 2009). The pressures and temperatures of the simulations reflect those of the phase equilibrium experiments. Corrected density adjusts the simulated density to account for small concentrations of $FeCO_3$ and SiO_2 present in the liquid produced in the original phase equilibrium experiments.

$MgCO_3$ (mol%)	Press. (GPa)	Temp. (K)	Gram formula wt.	Sim. Vol. (cm^3/mol)	Sim. ρ (g/cm^3)	Corrected ρ (g/cm^3)
Dalton and Wood (1993)						
13.6	1.5	1423	98.22	39.19	2.506	2.507
17.4	1.5	1423	97.69	39.23	2.490	2.497
22.5	2.2	1523	96.95	38.28	2.532	2.545
28.7	2.5	1523	96.05	37.76	2.544	2.558
31.6	2.8	1573	95.63	37.47	2.552	2.573
35.1	3.0	1573	95.11	37.09	2.564	2.585
Dalton and Presnall (1998)						
40.9	3.0	1518	93.64	36.59	2.559	2.561
44.0	3.5	1543	93.15	35.94	2.592	2.592
45.8	4.0	1563	92.86	35.44	2.620	2.618
49.2	5.0	1603	92.33	34.54	2.673	2.669
50.9	6.0	1653	92.05	33.77	2.726	2.717
55.5	7.0	1703	91.33	33.03	2.765	2.756
Hammouda (2003)						
10.5	6.0	1523	98.43	34.91	2.820	2.871
10.9	7.0	1273	98.36	33.61	2.927	2.957
10.8	10.0	1373	98.38	32.23	3.052	3.086
14.1	10.0	1473	97.86	32.47	3.014	3.068
Ghosh et al. (2009)						
87.1	12.5	1873	86.35	29.53	2.925	3.071
86.8	13.5	1823	86.40	29.12	2.967	3.096
61.1	15.0	1873	90.45	29.62	3.053	3.133
76.1	17.5	1833	88.08	28.30	3.112	3.182

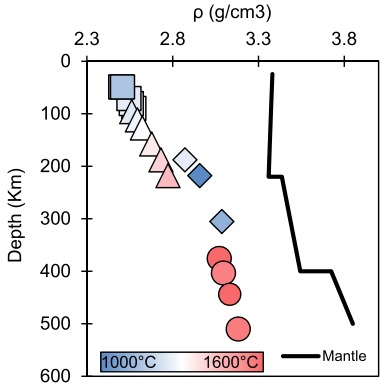

Fig. 6. The densities of primary carbonatite melts maintain a high negative density contrast with the surrounding mantle. The simulated densities of $MgCO_3$-$CaCO_3$ binary liquids representing primary carbonatite melts are corrected for minor $FeCO_3$ and SiO_2 concentration and are shown as a function of depth. The simulation temperatures, pressures and compositions are based on the phase equilibrium experiments of Dalton and Wood (1993) (squares), Dalton and Presnall (1998) (triangles), Hammouda (2003) (diamonds) and Ghosh et al. (2009) (circles). Coloring reflects simulation temperature. Mantle density as a function of depth is taken from PREM (Dziewonski and Anderson, 1981).

cosity of these kinds of liquids, any positive density contrast will swiftly drive liquid ascent; any degree of carbonate melt will thus quickly escape from a descending slab, inhibiting the subduction and storage of carbonate into the lower mantle.

The only common carbonate component heavy enough to potentially affect a density crossover in the mantle is $FeCO_3$ (which is a common component in mantle-derived carbonatite melts, e.g. Hammouda, 2003). Though our work does not directly address iron partitioning in carbonate-rich melts, we can use our model to approximate a minimum threshold iron-content that a hypothetical ferrocarbonatite must contain in order to affect a density crossover within the mantle. While $FeCO_3$ liquid was not directly simulated in this study, it's likely that $FeCO_3$ shares the volumetric properties of $MgCO_3$, since Fe^{2+} and Mg^{2+} have the same valence and similar ionic radii, and thus can frequently occupy the same atomic sites within crystal lattices and liquid pseudo-lattices. Assuming that $MgCO_3$ liquid molar volume is a reasonable proxy for $FeCO_3$, the $FeCO_3$ concentration necessary for affecting a density crossover can be calculated as a function of depth for a ferrocarbonatite in the $MgCO_3$-$CaCO_3$-$FeCO_3$ system. For the purposes of this calculation, it will be assumed that the molar volumes of all three components mix ideally and that $X^{Mg} = X^{Ca}$. The $MgCO_3$ & $FeCO_3$ liquid volumes are approximated at temperature and pressure using the thermodynamic properties presented this study (Table 1) in conjunction with Eqs. A.1-A.4.

The partial molar volume of the $CaCO_3$ liquid component is accurately estimated by combining experimental and theoretical constraints, using a 3rd order Birch-Murnaghan EOS with properties taken from the 1 bar molar volume model of Hurt and Lange (2019), the compressibility results of Hurt (2018) and the K' results from Hurt and Wolf (2018). The partial molar volume of the $MgCO_3$, $FeCO_3$ and $CaCO_3$ components were calculated at P-T conditions along an average carbonated peridotite solidus given by Dasgupta and Hirschmann (2010):

$$T\,(^{\circ}\mathrm{C}) = 0.0238 \times P^3 - 2.2084 \times P^2 \times 73.7991 \times P + 830.3808 \quad (4)$$

where P is in GPa. Using this approach, Fig. 7a shows the minimum requisite $FeCO_3$ concentration needed for a ferrocarbonatite to stagnate in the mantle gradually decreases through the upper mantle from a mol fraction of ~1 in the crust, to 0.5 (35 wt.% FeO) at the top of the transition zone. Throughout the transition zone, the threshold iron content is ~0.65 mol fraction $FeCO_3$. Such iron concentrations far exceed what's observed in phase equilibrium experiments on carbonated peridotite/eclogite (which generally produce carbonatite melts with <10 wt.% FeO). Fig. 7b shows

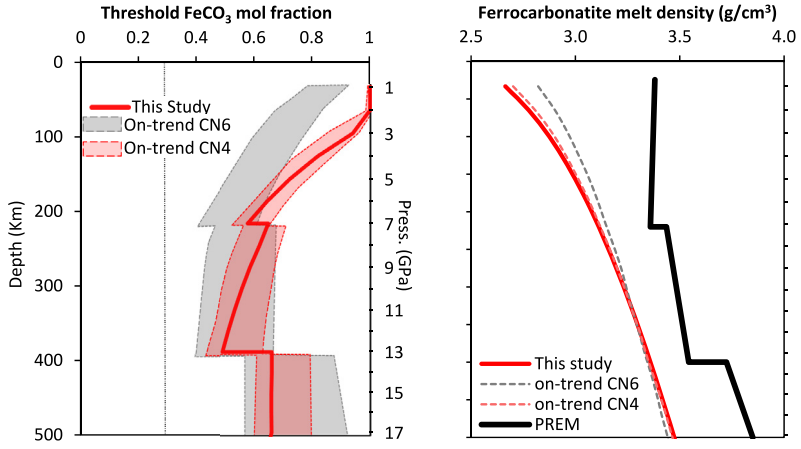

Fig. 7. Panel a shows the threshold mole percent $FeCO_3$ necessary for a hypothetical ferrocarbonatite (with composition $(Fe_x, Mg_{0.5\cdot(1-x)}, Ca_{0.5\cdot(1-x)})CO_3$) to achieve neutral buoyancy in the mantle as a function of depth. Three different estimates are depicted: the red line shows results from this study while the gray- and red-shaded regions represent estimated volumetric properties from Hurt (2018), which assume that both Mg^{2+} and Fe^{2+} are in 6-fold and 4-fold coordination with carbonate respectively. The dotted vertical dotted line shows the iron concentration of the only natural, unambiguously-magmatic ferrocarbonatite found in the literature (Thompson et al., 2002). Panel b shows the estimated densities of this natural ferrocarbonatite composition ($Fe_{0.26}$ $Mg_{0.22}$ $Ca_{0.52}$ CO_3) calculated for the three models (red lines are simulations from this study and the optimal on-trend CN6 and CN4 models from Hurt, 2018 are shown in gray- and red-dashed lines) along with the density of PREM (Dziewonski and Anderson, 1981).

the density of a melt with an approximate composition of a natural ferrocarbonatite (Thompson et al., 2002) which was calculated as a function of depth using the technique described above. As evident, its density remains consistently lower than the mantle through the transition zone.

It's difficult to assess with certainty whether significant volumes of such highly Fe-enriched (>40 mol% $FeCO_3$) ferrocarbonatites are actually produced in the mantle. After an exhaustive search of the literature, the ferrocarbonatite in Swartbooisdrif, Namibia (Thompson et al., 2002) appears to be the only natural ferrocarbonatite yet identified with an unambiguously magmatic origin. Thompson gives its composition as approximately $Fe_{0.26}$ $Mg_{0.22}$ $Ca_{0.52}$ CO_3. We find it interesting that the Swartbooisdrif ferrocarbonatite has a composition nearly identical to that of Ankerite, $Ca(Mg, Fe)(CO_3)_2$. If $FeCO_3$ behaves similarly to $MgCO_3$, we might expect an equilibrium liquid composition resulting from partial melting that is roughly equal parts Fe and Mg to be energetically favorable within the $FeCO_3$-$MgCO_3$-$CaCO_3$ ternary. Given the lack of natural samples, the energetic and volumetric properties predicted by our simulations, and the measured Fe-contents found in melting experiments on carbonated mantle materials, we find that ferrocarbonatites are unlikely to have sufficient Fe-enrichment to stagnate in the mantle owing to their large relative buoyancy.

5. Conclusions

We perform classical MD simulations of $MgCO_3$-bearing liquids using the empirical potential model of Hurt and Wolf (2018) at mantle pressures and temperatures. We find that $MgCO_3$ liquid assumes a novel topology characterized by four-fold coordination of Mg^{2+} with both the carbonate molecule and O^{2-}. Such a structure is markedly different from that of the other alkaline-earth carbonate liquids in which the metal cation is in 6-fold coordination with the carbonate molecule and 7-8 fold coordination with oxygen atoms. The liquid structure and resulting thermodynamic properties of $MgCO_3$ are found to be more similar to that of Li_2CO_3 than other alkaline-earth carbonate liquids, resulting in a dramatically more buoyant and compressible liquid than previous studies have suggested. The voluminous structure and subsequent low density of $MgCO_3$-rich liquids bolsters the density contrast of $MgCO_3$-bearing carbonatite melts in the mantle, increasing their already significant rates of ascent and preventing even relatively dense ferrocarbonatite melts from achieving a density crossover with the surrounding mantle.

The simulations have further suggested that $MgCO_3$ molar volume, thermal expansivity, compressibility, enthalpy and heat capacity do not mix ideally with (Ca, Sr, Ba)CO_3 liquids. Non-ideal mixing of volumetric properties stems from localized metal cation ordering around the Mg^{2+} ion. We find that it is energetically favorable to surround tetrahedral Mg-CO_3 complexes with octahedral Ca-, Sr-, Ba-carbonate complexes. This effect gradually diminishes with pressure, where $MgCO_3$ molar volume is found to mix near-ideally with $CaCO_3$-$SrCO_3$-$BaCO_3$ liquids by 12 GPa. On the other hand, non-ideal mixing of enthalpy in $MgCO_3$-bearing systems persists even at high pressure.

The novel topology of $MgCO_3$ liquid indicated by our simulations opens questions on another important component in mantle-derived carbonatite melts: $FeCO_3$. Given the similar ionic radii of Fe^{2+} and Mg^{2+}, it's possible that Fe^{2+} also assumes a 4-fold coordination with $(CO_3)^{2-}$ and O^{2-} in $FeCO_3$ liquid, producing a similar liquid structure to $MgCO_3$; the result would be a $FeCO_3$ component that is significantly less dense than what has been expected by other studies (e.g. Kang et al., 2016; Kang and Schmidt, 2017). Such a voluminous $FeCO_3$ component would inhibit ferrocarbonatite melts generated within subducting slabs from ever stagnating or sinking in the mantle, due to their low relative densities. Multi-angle energy dispersive X-ray diffraction experiments on $MgCO_3$- and $FeCO_3$-bearing melts are needed in order to verify the liquid structure of these important carbonate components.

Declaration of competing interest

The authors declare that they have no known competing financial interests or personal relationships that could have appeared to influence the work reported in this paper.

Acknowledgements

The authors would like to acknowledge Becky Lange, Udo Becker, Youxue Zhang and Will Bender, as well as two anonymous reviewers, for their helpful comments throughout the development of the research. S.H. and A.S.W. thank NSF-1763189 for primary financial support for this work, and S.H. also thanks the Rackham Merit Fellowship for additional financial support.

Appendix. Supplementary material

Supplementary material related to this article can be found online at https://doi.org/10.1016/j.epsl.2019.115927.

References

Berendsen, H.J.C., Postma, J.P.M., Van Gunsteren, W.F., Di Nola, A., Haak, J.R., 1984. Molecular dynamics with coupling to an external bath. J. Chem. Phys. 81, 3684–3690.

Berman, R.G., Brown, T.H., 1985. Heat capacity of minerals in the system Na_2O-K_2O-CaO-MgO-FeO-Fe_2O_3-Al_2O_3-SiO_2-TiO_2-H_2O-CO_2: representation, estimation, and high temperature extrapolation. Contrib. Mineral. Petrol. 89, 168–183.

Biellmann, C., Gillet, P., Guyot, F., Peyronneau, J., Reynard, B., 1993. Experimental evidence for carbonate stability in the Earth's lower mantle. Earth Planet. Sci. Lett. 118, 31–41.

Blundy, J., Dalton, J., 2000. Experimental comparison of trace element partitioning between clinopyroxene and melt in carbonate and silicate systems, and implications for mantle metasomatism. Contrib. Mineral. Petrol. 139, 356–371.

Cormier, L., Cuello, G.J., 2013. Structural investigation of glasses along the $MgSiO_3$-$CaSiO_3$ join: diffraction studies. Geochim. Cosmochim. Acta 122, 498–510.

Dalton, J.A., Presnall, D.C., 1998. Carbonatitic melts along the solidus of model lherzolite in the system CaO-MgO-Al_2O_3-SiO_2-CO_2 from 3 to 7 GPa. Contrib. Mineral. Petrol. 131, 123–135.

Dalton, J.A., Wood, B.J., 1993. The compositions of primary carbonate melts and their evolution through wallrock reaction in the mantle. Earth Planet. Sci. Lett. 119, 511–525.

Dasgupta, R., Hirschmann, M.M., 2006. Melting in the Earth's deep upper mantle caused by carbon dioxide. Nature 440, 659–662.

Dasgupta, R., Hirschmann, M.M., 2010. The deep carbon cycle and melting in Earth's interior. Earth Planet. Sci. Lett. 298, 1–13.

Dasgupta, R., Hirschmann, M.M., Stalker, K., 2006. Immiscible transition from carbonate-rich to silicate-rich melts in the 3 GPa melting interval of eclogite + CO2 and genesis of silicaundersaturated ocean island lavas. J. Petrol. 47, 647–671.

Datta, R.K., Roy, D.M., Faile, S.P., Tuttle, O.F., 1964. Glass formation in carbonate systems. J. Am. Ceram. Soc. 47, 153. https://doi.org/10.1111/j.1151-2916.1964.tb14377.x.

Dziewonski, A.M., Anderson, D., 1981. Preliminary reference Earth model. Phys. Earth Planet. Inter. 25, 297–356.

Ganster, P., Benoit, M., Delaye, J.M., Kob, W., 2007. Structural and vibrational properties of a calcium aluminosilicate glass: classical force-fields vs. first-principles. Mol. Simul. 33, 1093–1103.

Genge, M.J., Price, G.D., Jones, A.P., 1995. Molecular dynamics simulations of $CaCO_3$ melts to mantle pressures and temperatures: implications for carbonatite magmas. Earth Planet. Sci. Lett. 131, 225–238.

Ghiorso, M.S., Hirschmann, M.M., Reiners, P.W., Kress, V.C., 2002. The pMELTS: a revision of MELTS for improved calculation of phase relations and major element partitioning related to partial melting of the mantle to 3 GPa. Geochem. Geophys. Geosyst. 3, 36.

Ghosh, D.B., Bajgain, S.K., Mookherjee, M., Karki, B.B., 2017. Carbon-bearing silicate melt at deep mantle conditions 7, 848.

Ghosh, S., Ohtani, E., Litasov, K.D., Terasaki, H., 2009. Solidus of carbonated peridotite from 10 to 20 GPa and origin of magnesiocarbonatite melt in the Earth's deep mantle. Chem. Geol. 262, 17–28.

Green, D.H., Wallace, M.E., 1988. Mantle metasomatism by ephemeral carbonatite melts. Nature 336, 459–462.

Guillot, B., Sator, N., 2007. A computer simulation study of natural silicate melts. Part II: high pressure properties. Geochim. Cosmochim. Acta 71, 4538–4556.

Hammouda, T., 2003. High-pressure melting of carbonated eclogite and experimental constraints on carbon recycling and storage in the mantle. Earth Planet. Sci. Lett. 214, 357–368.

Hoover, W.G., 1985. Canonical dynamics: equilibrium phase-space distributions. Phys. Rev. A 31, 1695–1697.

Hudspeth, J., Sanloup, C., Kono, Y., 2018. The properties of molten $CaCO_3$ at high pressure. Geochem. Perspect. Lett. 7, 17–21.

Hurst, H.J., 1991. The thermal decomposition of magnesite in nitrogen. Thermochim. Acta 189, 91–96.

Hurt, S.M., 2018. The Thermodynamic Properties and Structure of Alkali and Alkaline Earth Carbonate Melts. PhD thesis. University of Michigan, Ann Arbor.

Hurt, S.M., Lange, R.A., 2019. The density of Li_2CO_3-Na_2CO_3-K_2CO_3-Rb_2CO_3-Cs_2CO_3-$CaCO_3$-$SrCO_3$-$BaCO_3$ liquids: new measurements, ideal mixing, and systematic trends with cation coordination. Geochim. Cosmochim. Acta 248, 123–137.

Hurt, S.M., Wolf, A.S., 2018. Thermodynamic properties of $CaCO_3$-$SrCO_3$-$BaCO_3$ liquids: a molecular dynamics study using new empirical atomic potentials for alkaline earth carbonates. Phys. Chem. Miner. https://doi.org/10.1007/s00269-018-0995-5.

Irving, A.J., Wyllie, P.J., 1975. Subsolidus and melting relationships for calcite, magnesite and the join $CaCO_3$-$MgCO_3$ 36 kb. Geochim. Cosmochim. Acta 39, 35–53.

Kang, N., Schmidt, M.W., 2017. The melting of subducted banded iron formations. Earth Planet. Sci. Lett. 476, 165–178.

Kang, N., Schmidt, M.W., Poli, S., Connolly, J.A.D., Franzolin, E., 2016. Melting relations in the system $FeCO_3$-$MgCO_3$ and thermodynamic modelling of Fe-Mg carbonate melts. Contrib. Mineral. Petrol. 171, 1–16.

Karki, B.B., Ghosh, D.B., Bajgain, S.K., 2018. Simulation of silicate melts under pressure. In: Kono, Y., Sanloup, C. (Eds.), Magmas Under Pressure: Advances in High-Pressure Experiments on Structure and Properties of Melts. Elsevier, Cambridge, pp. 419–453.

Katsura, T., Ito, E., 1990. Melting and subsolidus phase relations in the $MgSiO_3$-$MgCO_3$ system at high pressures: implications to evolution of the Earth's atmosphere. Earth Planet. Sci. Lett. 99, 110–117.

Kono, Y., Kenney-Benson, C., Hummer, D., Ohfuji, H., Park, C., Shen, G., Wang, Y., Kavner, A., Manning, C.E., 2014. Ultralow viscosity of carbonate melts at high pressures. Nat. Commun. 5, 5091.

Kroeker, S., Stebbins, J.F., 2000. Magnesium coordination environments in glasses and minerals: new insight from high-field magnesium-25 MAS NMR. Am. Mineral. 85, 1459–1464.

Kubicki, J.D., Hemley, R.J., Hofmeister, A.M., 1992. Raman and infrared study of pressure-induced structural changes in $MgSiO_3$, $CaMgSi_2O_6$, and $CaSiO_3$ glass. Am. Mineral. 77, 258–262.

Lange, R.A., 1997. A revised model for the density and thermal expansivity of K_2O-Na_2O-CaO-MgO-Al_2O3-SiO_2 liquids from 700 to 1900 K: extension to crustal magmatic temperatures. Contrib. Mineral. Petrol. 130, 1–11.

Li, Z., Li, J., Lange, R., Liu, J., Militzer, B., 2017. Determination of calcium carbonate and sodium carbonate melting curves up to Earth's transition zone pressures with implications for the deep carbon cycle. Earth Planet. Sci. Lett. 457, 395–402.

Liu, Q., Lange, R.A., 2003. New density measurements on carbonate liquids and the partial molar volume of the $CaCO_3$ component. Contrib. Mineral. Petrol. 146, 370–381.

Morizet, Y., Trcera, N., Larre, C., Rivoal, M., Le Menn, E., Vantelon, D., Gaillard, F., 2019. X-ray absorption spectroscopic investigation of the Ca and Mg environments in CO_2-bearing silicate glasses. Chem. Geol. 510, 91–102.

Nosé, S., 1984. A unified formulation of the constant temperature molecular dynamics methods. J. Chem. Phys. 81, 511.

O'Leary, M.C., Lange, R.A., Ai, Y., 2015. The compressibility of $CaCO_3$-Li_2CO_3-Na_2CO_3-K_2CO_3 liquids: application to natrocarbonatite and CO_2-bearing nephelinite liquids from Oldoinyo Lengai. Contrib. Mineral. Petrol. 170, 1–18.

Plimpton, S., 1995. Fast parallel algorithm for short-range molecular dynamics. J. Comput. Phys. 117, 1–42.

Powell, R., Holland, T.J.B., 1988. An internally consistent dataset with uncertainties and correlations: 3. Applications to geobarometry, worked examples and a computer program. J. Metamorph. Geol. 62, 173–204.

Ragone, S.E., Datta, R.K., Roy, D.M., Tuttle, O.F., 1966. The system potassium carbonate—magnesium carbonate. J. Phys. Chem. 70, 3360–3361. https://doi.org/10.1021/j100882a515.

Roest, D.L., Ballone, P., Bedeaux, D., Kjelstrup, S., 2017. Molecular dynamics simulations of metal/molten alkali carbonate interfaces. J. Chem. Phys. C. 121, 17827–17847.

Roy, R., 1950. Magnesium in fourfold coordination in glass. J. Am. Chem. Soc. 72, 3307–3308.

Sharma, S.K., Simons, B., 1980. Raman study of K_2CO_3-$MgCO_3$ glasses. In: Carnegie Institute of Washington Yearbook, vol. 79, pp. 322–326.

Shimoda, K., Nemoto, T., Saito, K., 2008. Local structure of magnesium in silicate glasses: a ^{25}Mg 3QMAS NMR study. J. Phys. Chem. B 112, 6747–6752.

Solomatova, N.V., Caracas, R., Manning, C.E., 2019. Carbon sequestration during core formation implied by complex carbon polymerization. Nat. Commun. 10, 789.

Staudigel, H., Hart, S.R., Schmincke, H.U., Smith, B.M., 1989. Cretaceous ocean crust at DSDP Sites 417 and 418: carbon uptake from weathering versus loss by magmatic outgassing. Geochim. Cosmochim. Acta 53, 3091–3094.

Thompson, R., Smith, P., Gibson, S., Mattey, D., Dickin, A., 2002. Ankerite carbonatite from Swartbooisdrif, Namibia: the first evidence for magmatic ferrocarbonatite. Contrib. Mineral. Petrol. 143, 377–396.

Trcera, N., Cabaret, D., Rossano, S., Farges, F., Flank, A.M., Lagarde, P., 2009. Experimental and theoretical study of the structural environment of magnesium in minerals and silicate glasses using X-ray absorption near-edge structure. Phys. Chem. Miner. 36, 241–257.

Vuilleumier, R., Seitsonen, A., Sator, N., Guillot, B., 2014. Structure, equation of state and transport properties of molten calcium carbonate ($CaCO_3$) by atomistic simulations. Geochim. Cosmochim. Acta 141, 547–566.

Waseda, Y., Toguri, J.M., 1977. The structure of molten binary silicate systems CaO-SiO_2 and MgO-SiO_2. Metall. Mater. Trans. B 8, 563–568. https://doi.org/10.1007/BF02669331.